Charge oscillations in coupled quantum wells

C. Juang
C.B. Tsai
J. Juang

Indexing terms: Coherent tunnelling, Coupled quantum wells

Abstract: A study of charge oscillations due to electron- and hole-coherent, and mixing tunnelling in coupled quantum well structures is given. The time-dependent picture of coherent tunnelling of an electron and hole wave packet is obtained by the application of the time-development operator of the time-dependent Schrödinger equation, and the time-dependent Schrödinger equation with the Luttinger Hamiltonian. Detailed physical mechanisms involving resonant coherent tunnelling on electrons, valence-band mixing effects on heavy- and light-hole tunnelling, spatial and mixing multiple tunnelling effects, in coupled quantum wells are described.

1 Introduction

The possibility of utilising interwell coherent tunnelling in coupled quantum wells which consist of two quantum wells located sufficiently close together was first proposed by Luryi in 1988 [1, 2]. For a particle initially confined in one of the wells, interwell tunnelling occurs with an applied field. If the energy states in both wells are far apart, the tunnelling is nonresonant type. If the energy states in both wells are very close to each other, resonant tunnelling occurs. By changing the external electric field across coupled quantum wells, the resonant condition can be achieved. At resonance, high-speed oscillations for both electrons and holes occur between these two wells. Considerable efforts have been devoted to this oscillation effects owing to its rich physical nature and possible device applications [3–17].

In the case of electron spatial tunnelling, tunnelling time from one well to the other well at nonresonance has been measured [3]. By applying an external electric field across coupled quantum wells, the resonant condition can be achieved and a significant difference in tunnelling time has been observed using luminescence spectroscopy [4–6]. In addition, a real-time coherent oscillation of an electron wave packet in a coupled quantum well structure has been reported using the pump and probe technique and the time-domain terahertz spectroscopy [7, 8]. This oscillatory motion of the wave package is shown to be strongly influenced by the external bias voltage (see review by Brener *et al.* [9]).

In the case of the hole tunnelling in the coupled quantum wells, the mechanisms are significantly complicated owing to band mixing effects [10–17]. Two possible mechanisms: spatial tunnelling (from one well to the other) and mixing tunnelling (between heavy (HH) and light hole (LH) states) are involved in the process. It has been shown that heavy-to-light hole mixing tunnelling is less effective compared with heavy-hole spatial tunnelling [10]. However, some theoretical studies have suggested the importance of band mixing effects in hole tunnelling in coupled wells and double barrier structures [11–13]. Several experiments also point to the significance of band-mixing effects on the spatial and mixing tunnelling of the heavy hole in coupled quantum wells [14–17].

Electron-coherent tunnelling in coupled quantum wells has been described by the application of the time-development operator according to the time-dependent Schrödinger equation [18, 19]. Resonant tunnelling effects have been shown while the energy states in both wells are very close to each other. In addition, the tunnelling of a probability density function at resonance and nonresonance can be described in real time. Spatial hole tunnelling and mixing has been described using the time-dependent Schrödinger equation with the Luttinger Hamiltonian [20]. In this approach, valence-band mixing is taken into consideration by the Luttinger Hamiltonian. Thus, mixing tunnelling and spatial tunnelling which happen at the same time, can be clearly resolved.

2 Numerical analysis

2.1 Analysis of electron tunnelling

To show the field-induced interwell coherent tunnelling in coupled quantum wells the evolution of a one-dimensional envelope wavefunction $\phi(x, t)$ is determined by the time-dependent Schrödinger equation

$$H\phi(x,t) = i\hbar\frac{\partial}{\partial t}\phi(x,t) \tag{1}$$

with BenDaniel and Duke's effective Hamiltonian

$$H = \frac{-\hbar^2}{2}\frac{\partial}{\partial x}\left(\frac{1}{m^*(x)}\frac{\partial}{\partial x}\right) + V(x) \tag{2}$$

so as to preserve the continuity of the wavefunction. The additional potential $|e|Fx$ due to the external electric field is added directly to the potential profile of the coupled quantum well structure. Eqn. 1 can be

IEE Proceedings online no. 19960830

Paper first received 12th April 1996 and in revised form 13th August 1996

C. Juang is with the Electronics Department, Ming Hsin College of Technology, Hsinchu, Taiwan 300, Republic of China

C.B. Tsai and J. Juang are with the Department of Applied Mathematics, National Chiao Tung University, Hsinchu, Taiwan 300, Republic of China

discretised with respect to time and space [18]

$$\frac{\phi_{j+1,n+1}}{m^*_{j+1}+m^*_j}+\left(\frac{2\epsilon^2}{\hbar\delta}i-\frac{\epsilon^2}{\hbar^2}V_j-\frac{1}{m^*_{j+1}+m^*_j}-\frac{1}{m^*_{j-1}+m^*_j}\right)\times\phi_{j,n+1}+\frac{\phi_{j-1,n+1}}{m^*_{j-1}+m^*_j}+\frac{\phi_{j+1,n}}{m^*_{j+1}+m^*_j}-\left(\frac{2\epsilon^2}{\hbar\delta}i+\frac{\epsilon^2}{\hbar^2}V_j+\frac{1}{m^*_{j+1}+m^*_j}+\frac{1}{m^*_{j+1}+m^*_j}\right)\phi_{j,n}+\frac{\phi_{j-1,n}}{m^*_{j-1}+m^*_j}=0, \tag{3}$$

where ε, j, δ, and n are the space interval, space index, time interval and time index, respectively. In the numerical calculations the space interval ε and time interval δ are chosen to be 1Å and 1 femtosecond (10^{-15}). With an initial wavefunction, eqn. 3 can be reduced to a standard $Ax = b$ matrix equation with A being a complex tridiagonal matrix. This matrix equation is solved by the Gaussian elimination method and time evolution can be obtained by iterative multiplication of the inverted matrix.

2.2 Hole mixing and spatial tunnellings

The time-dependent Schrödinger equation with the reduced 2 × 2 Luttinger Hamiltonian H_h is written as [20, 21]

$$\begin{pmatrix} P+Q+V_h(z) & \tilde{R} \\ \tilde{R}^* & P-Q+V_h(z) \end{pmatrix}\begin{pmatrix}\phi^1(x,t)\\ \phi^2(x,t)\end{pmatrix} = i\hbar\frac{\partial}{\partial t}\begin{pmatrix}\phi^1(x,t)\\ \phi^2(x,t)\end{pmatrix} \tag{4}$$

where

$$P=\frac{1}{2}\left(\frac{\hbar^2}{m_0}\right)\gamma_1 k_{||}^2-\frac{1}{2}\left(\frac{\hbar^2}{m_0}\right)\frac{\partial}{\partial z}\gamma_1\frac{\partial}{\partial z}$$

$$Q=\frac{1}{2}\left(\frac{\hbar^2}{m_0}\right)\gamma_2 k_{||}^2+\left(\frac{\hbar^2}{m_0}\right)\frac{\partial}{\partial z}\gamma_2\frac{\partial}{\partial z} \tag{5}$$

$$\tilde{R}=\left(\frac{\hbar^2}{m_0}\right)\left(\frac{\sqrt{3}}{4}(\gamma_2+\gamma_3)k_{||}^2-\frac{\sqrt{3}}{2}k_{||}\left(\gamma_3\frac{\partial}{\partial z}+\frac{\partial}{\partial z}\gamma_3\right)\right)$$

and $\phi^1(x, t)$ and $\phi^2(x, t)$ are HH and LH state envelope wavefunctions, respectively, γ_1, γ_2, γ_3 are the Luttinger parameters and are position-dependent in the heterojunction structures, m_0 is the electron rest mass, the inplane vector $k_{||}^2 = k_x^2 + k_y^2$. The discretisation of eqn. 1 with respect to time gives [20]

$$\left(1+\frac{i\delta}{2\hbar}H_h\right)\begin{pmatrix}\phi^1_{n+1}\\ \phi^2_{n+1}\end{pmatrix}=\left(1-\frac{i\delta}{2\hbar}H_h\right)\begin{pmatrix}\phi^1_{n}\\ \phi^2_{n}\end{pmatrix} \tag{6}$$

where δ and n are the time spacing and time index, respectively. This discrete-time technique preserves normalisation of the wave function and introduces no extra nonlinear effect to the system. This difference equation can be written in a linear $Ax = b$ matrix equation with A being a complex symmetry matrix. The matrix is then solved using the L-U decomposition technique. Asymmetric coupled quantum well systems of 25–15–49 (first well width–barrier width–second well width in Angstroms) with a barrier height of 0.2506eV are investigated. In this structure the HH state in the first well is aligned with the LH state in the second well. The Luttinger parameters (γ_1, γ_2, γ_3) are chosen to be (6.85, 2.1, 2.9) in the well region and (5.15, 1.39, 2.10), which are obtained by a linear interpolation of the Luttinger parameters of GaAs and AlAs, in the barrier region. Also, the space interval ε and time interval δ are chosen to be 1Å and 1 femtosecond (10^{-15}). The initial wave functions are the heavy-hole wave functions in the first well, and the tunnelling process is initiated at $t = 0$ without any driven force.

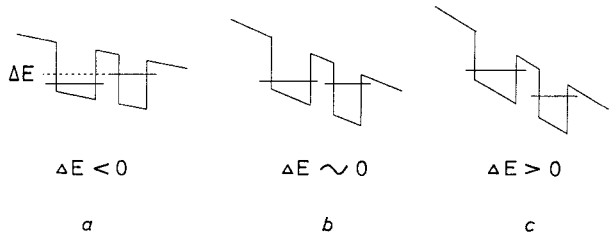

Fig. 1 *Schematic potential profiles of coupled quantum wells under external electric field at resonance and off-resonance*
a Off resonance
b Resonance
c Off resonance

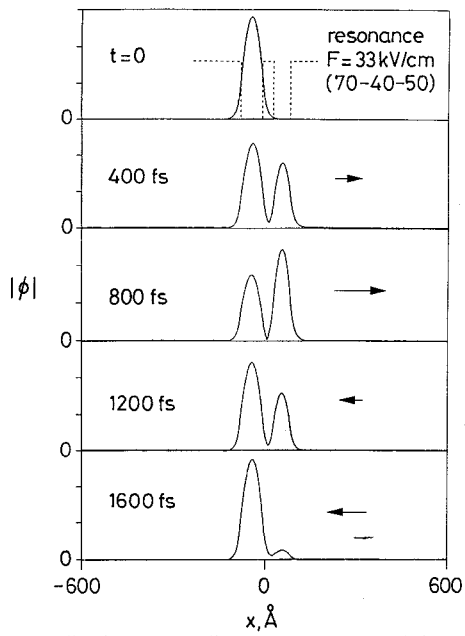

Fig. 2 *Interwell coherent tunnelling in 70–40–50 coupled quantum wells subject to an external electric field of 33kV/cm (resonance)*
Position of coupled quantum wells is shown by dotted line at $t = 0$ frame
Arrows indicate oscillation of wave packet
At 400 and 800fs the wave packet tunnels into second well while at 1200 and 1600 wave packet tunnels back to first well

3 Electron tunnelling

3.1 Wave package

Coupled quantum well systems of 70–40–50 with barrier height of 0.4eV are studied. The effective masses are 0.067 m_0 in well region and 0.1002 m_0 in barrier region. The energy difference ΔE is given by [18]

$$\Delta E = E_{1F} - E_{2F} + F\left(p+\frac{1+q}{2}\right) \tag{7}$$

where l, p, and q denote the first well width, barrier width, and second well width in coupled quantum wells, respectively, E_{1F} and E_{2F} are the ground energy states in the first and second wells, respectively, assuming that two wells are isolated from each other, and F is the external electric field. An external electric field of 33kV/cm corresponding to the resonant conditions between the two wells is chosen. Fig. 1 illustrates resonance in coupled quantum wells owing to the external electric field. The initial wavefunction is the eigenfunction of the first well without the electric field, and the tunnelling process is initiated by the onset of an applied electric field. This provides a detailed time-dependent picture of field-induced coherent tunnelling in coupled quantum wells. In Fig. 2 the wave packet

tunnels from the first well to the second well during the first 800fs. However, as time increases the wave packet tunnels back to the first well. The arrows indicate the oscillation of the wave packet.

3.2 Tunnelling probability

To further characterise the properties of interwell tunnelling based on time-dependent analysis and to show the effects of the barrier width, the tunnelling probability $P(t)$ (which represents the tunnelling of a particle after a time t since the initialisation of the tunnelling process) can be defined using the overlap integral between two wavefunctions as [18]

$$P(t) = 1 - |\langle\phi(x,0)|\phi(x,t)\rangle|^2 \quad (8)$$

Fig. 3 shows the tunnelling probability at resonance for 70–30–50 (F = 36.7kV/cm), 70–40–50 (F = 33kV/cm), and 70–50–50 (F = 30kV/cm) coupled quantum well systems. The electric fields for these three cases are chosen so that ΔEs are close (–0.475, –0.478, and –0.458meV, respectively). In all cases, the particle tunnels into the second well very rapidly at the beginning. The tunnelling process seems to slow down and then the particle slowly tunnels back to the first well. Again, the particle tunnels into the second well very rapidly as the beginning of the tunnelling process. There is a very significant difference between tunnelling into the second well and tunnelling back to the first well. This shows that field-induced interwell coherent tunnelling possesses an asymmetric oscillation effect.

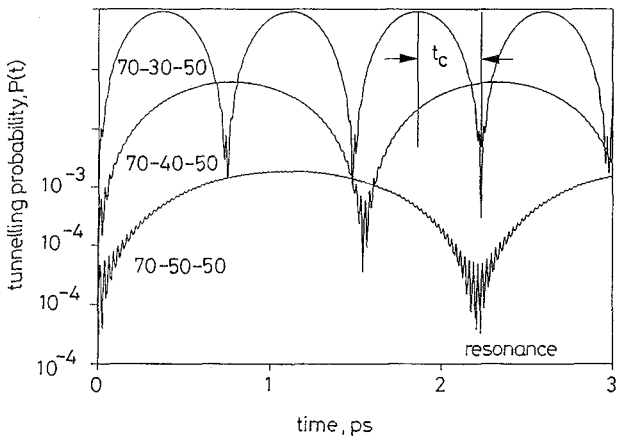

Fig. 3 *Tunnelling probability defined by eqn. 10 for coupled quantum wells with various barrier width at resonance*
Applied electric fields are 36.7, 33, and 30kV/cm corresponding to ΔEs of –0.475, –0.478, and –0.46meV for 70–30–50, 70–40–50, and 70–50–50 coupled quantum wells, respectively

In addition, Fig. 3 shows some properties and their dependence on the barrier width for close $|\Delta E|$s. For a narrow barrier width (70–30–50), the tunnelling cycle is shorter and the maximum tunnelling probability is larger. This indicates that for a narrow barrier it takes a shorter time to tunnel through and a larger portion of the wave packet is involved in the tunnelling process. Another interesting property associated with the coherent tunnelling effect in coupled quantum wells is the peak-to-valley ratio of the tunnelling probability, which characterises the amplitude of the oscillation. The typical peak to valley ratios for 70–30–50, 70–40–50, and 70–50–50 at resonance are 6.27, 3.58, and 2.45 $\times$ 10^2. A narrow barrier also gives a larger peak-to-valley ratio.

3.3 Effects of barrier width

The oscillation frequency can be defined as the inverse of a tunnelling cycle T, which is the time required for the tunnelling probability $P(t)$ to reach from a local maximum to next local maximum in Fig. 3. Fig. 4 shows resonant oscillation frequency as a function of barrier width b in 70–b–70 symmetric coupled wells. As the barrier width increases, oscillation frequency decreases. A very strong (almost exponential) dependence of oscillation frequency on the barrier width is shown. This agrees quite well with the conventional model in which the tunnelling probability is a function of exp(–αb), where b is the barrier width. However, as the barrier width increases (two wells are decoupled), this almost-exponential dependence of the oscillation frequency seems to be weakened in the time-dependent model.

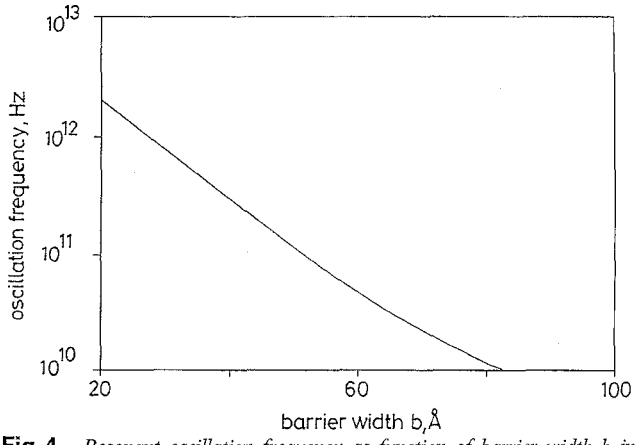

Fig. 4 *Resonant oscillation frequency as function of barrier width b in 70–b–70 symmetric coupled wells*

4 Hole mixing and spatial tunnellings

4.1 Wave package

Coupled quantum well systems of 25–15–25 with a barrier height of 0.2506eV, which corresponds to a 50% of Al content in an AlGaAs/GaAs system with a 60:40 ratio of ΔE_c to ΔE_v are investigated. The Luttinger parameters (γ_1, γ_2, γ_3) are chosen to be (6.85, 2.1, 2.9) in the well region and (5.15, 1.39, 2.10), which are obtained by a linear interpolation of the Luttinger parameters of GaAs and AlAs in the barrier region [21]. In-plane wave vector $k_{\|}$ is chosen to be 0.02 ($2\pi/a$), where a is the lattice constant of GaAs. The initial wavefunctions are the heavy and light hole wavefunctions in the first well and the tunnelling process is initiated at t = 0.

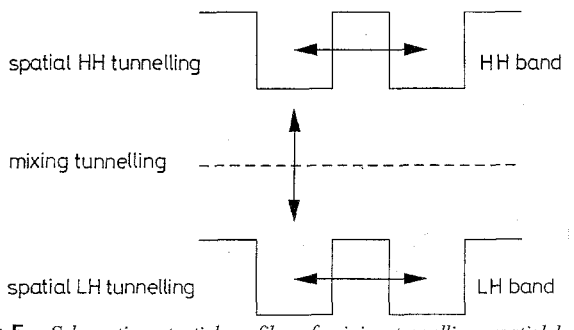

Fig. 5 *Schematic potential profiles of mixing tunnelling, spatial heavy hole tunnelling, and spatial light-hole tunnelling in light and heavy-hole bands of coupled quantum wells with band-mixing effects*

An illustration of spatial tunnelling (from one well to the other) and mixing tunnelling (between heavy- and light-hole states) is given in the Fig. 5. With this

nonzero inplane wave vector $k_{||}$, heavy- and light-hole wavefunctions are mixed together as the tunnelling process goes on. So, spatial light-hole tunnelling is possible when a pure heavy-hole wave packet is used as initial function, and *vice versa*.

Fig. 6 shows the interwell tunnelling of heavy hole and light hole in 25–15–25Å coupled quantum wells. The initial wavefunction is the eigenfunction of the first well. In Fig. 6, the heavy-hole wave packet tunnels from the first well to the second well during the first 215fs. However, as time increases the wave packet tunnels back to the first well. As shown, a larger portion of the wave packet is involved in this tunnelling process. At the same time, the wave packet also oscillates between the heavy-hole band and light-hole band, where there is no wave package in light-hole band at $t = 0$.

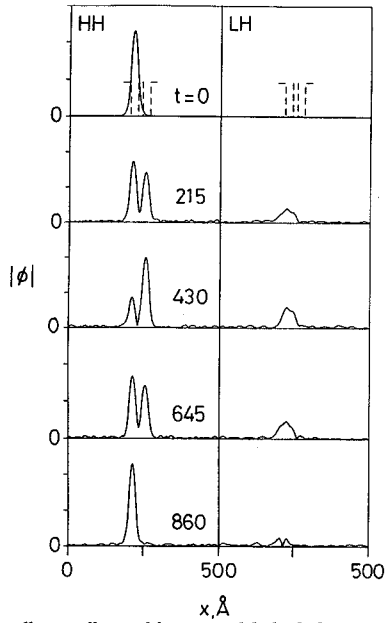

Fig. 6 *Interwell tunnelling of heavy and light holes in 25–15–25Å coupled quantum wells with band mixing ($k_{||}$ = 0.02)*
Position of coupled quantum wells is shown by dotted line at $t = 0$ frame

4.2 Mixing tunnelling

Mixing tunnelling occurs between heavy- and light-hole states owing to band mixing effects. To characterise the properties of the mixing tunnelling based on the time-dependent analysis one can define a probability factor $F(t)$ as the probability of finding the heavy hole in the heavy-hole band [20]

$$F(t) = \int_{hh} \phi^1(x,t)\phi^{1*}(x,t)dx \qquad (9)$$

where $\phi^1(x, t)$ is the heavy hole wavefunction. When $F(t)$ approaches one, the wave packet is mainly located in the heavy hole band. When $F(t)$ is small, the wave packet has left the heavy-hole band and tunnels into the light-hole band. Therefore the oscillation frequency and amplitude of the mixing tunnelling can be fully described by this probability factor $F(t)$.

Fig. 7 shows $F(t)$ as a function of time for HH to LH tunnelling. For a pure heavy hole (no probability at light hole band), F is equal to one at the beginning, as indicated by HH initial. As time passes, it is shown that the wave packet oscillates between the heavy-hole band and light-hole band with a high oscillation frequency and a small oscillation amplitude. This indicates that it takes a short time to tunnel between heavy- and light-hole states, and only a small portion of the wave packet is involved in the tunnelling process (less than 25% wave packet found in the light hole band at maximum). For a pure light hole (LH to HH), as indicated by LH initial, the tunnelling cycle is longer and the amplitude is larger, meaning that a larger portion of the wave packet is involved in the tunnelling process (more than 60% wave packet found in the heavy hole band at maximum). This suggests that light-to-heavy hole is more effective in the mixing tunnelling.

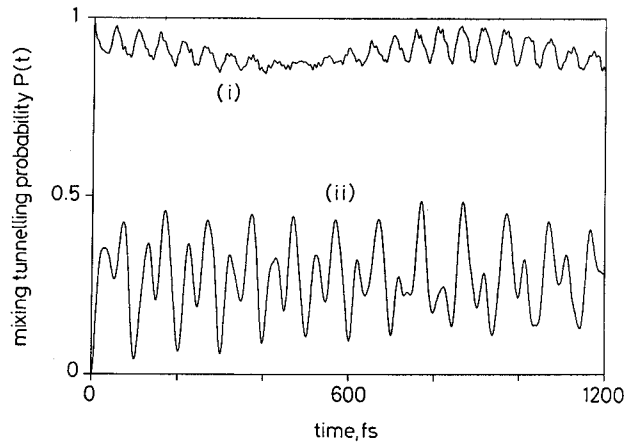

Fig. 7 *Mixing tunnelling probability factor $F(t)$ defined by eqn. 8 as function of time for heavy hole (HH initial) and light hole (LH initial) as initial wave packets in 25–15–25Å coupled quantum wells with band mixing ($k_{||}$ = 0.02 ($2\pi/a$))*
(i) HH initial
(ii) LH initial

4.3 Spatial hole tunnelling

Spatial tunnelling occurs between the first and the second wells in both heavy-hole band and light-hole band. In the absence of band mixing effects ($k_{||} = 0$), spatial tunnelling is similar to that in the conduction band. However, by taking band mixing effects into consideration, the tunnelling process is significantly affected by band-mixing effects. Using the same definition of the tunnelling probability, Fig. 8 shows $P(t)$ of the heavy-hole wavefunction, which describes the spatial heavy-hole tunnelling.

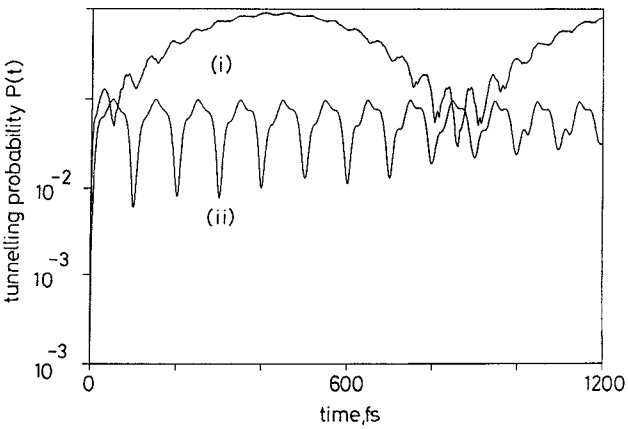

Fig. 8 *Spatial tunnelling probability of heavy hole as a function of time using heavy hole (HH initial) and light hole (LH initial) as initial wave packet in 25–15–25Å coupled quantum wells with band mixing ($k_{||}$ = 0.02 ($2\pi/a$))*
(i) HH initial
(ii) LH initial

For a pure initial heavy hole (HH initial), the heavy-hole wave packet undergoes spatial tunnelling and mixing tunnelling (from heavy to light-hole band) at the same time. However, the heavy to light-hole tunnelling is less effective in the mixing tunnelling. Thus, spatial tunnelling is dominant and the ripples in the $P(t)$ result from the modulation of the mixing tunnelling. For a pure initial light hole, there is no wave packet in the

heavy-hole band in the beginning. Due to the mixing tunnelling, the particle tunnels into the heavy-hole band and proceeds to spatial tunnelling. The light- to-heavy hole mixing tunnelling is very effective. Thus, a noticeable heavy-hole spatial tunnelling occurs even though there is no wave packet in the heavy-hole band before tunnelling.

4.4 Effects of $k_{||}$

The effect of band mixing as a function of k is further described in Figs. 9 and 10. For a small k there is only spatial tunnelling in Fig. 9. As k is increased the mixing effects are enhanced. The mixing tunnelling becomes clear around $k = 0.02$ and become dominant beyond $k = 0.025$. Also, the band-mixing effects slow down the HH spatial tunnelling process as the spatial oscillation period becomes larger if a pure initial heavy-hole wave packet is used. The same effect of slowing down is also true for mixing tunnelling (HH to LH) although the effect is less sensitive.

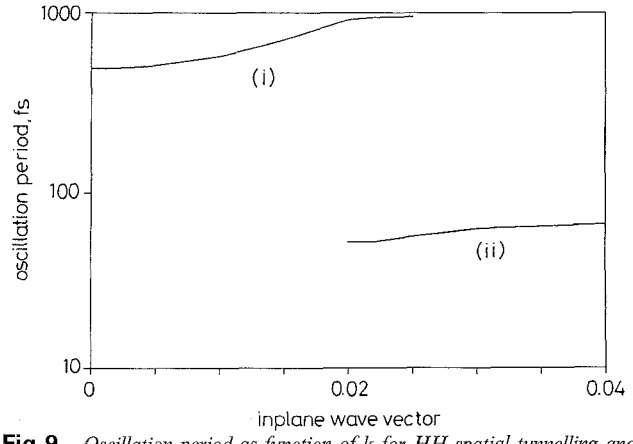

Fig. 9 *Oscillation period as function of k for HH spatial tunnelling and HH-to-LH mixing tunnelling in 25–15–25 Å coupled quantum wells*
(i) spatial
(ii) mixing

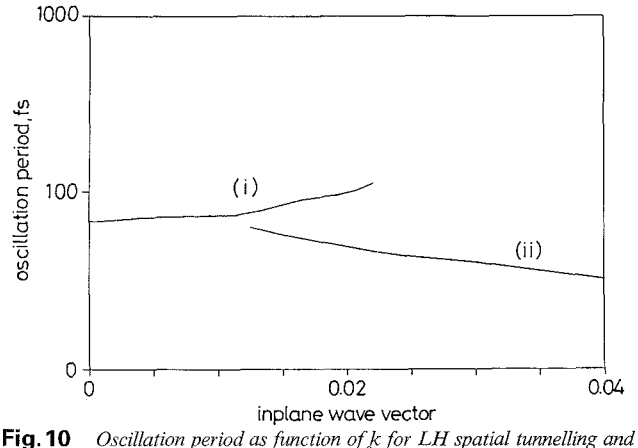

Fig. 10 *Oscillation period as function of k for LH spatial tunnelling and LH-to-HH mixing tunnelling in 25–15–25 Å coupled quantum wells*
(i) spatial
(ii) mixing

For a pure initial light hole (Fig. 10), the k also indicates three distinguishable areas: spatial-dominant ($k < 0.01$), transition ($0.01 < k < 0.025$), and mixing-dominant ($k > 0.025$). Also, the band-mixing effects slow down the LH spatial tunnelling process as the spatial oscillation period becomes larger. However, the mixing tunnelling (LH to HH) becomes much faster as k increases. This also supports that the light to heavy-hole mixing tunnelling is much effective than that of HH hole to light hole tunnelling.

5 Conclusions

Compared with time-independent analysis, the method presented in this work offers a better picture of electron resonant tunnelling, hole mixing tunnelling, and spatial heavy and light-hole tunnelling in coupled quantum wells. Time evolution of the heavy- and light-hole wave packet in the coupled quantum wells with band-mixing effects was shown by a numerical implementation of the time-development operator of the Schrödinger equation with the Luttinger Hamiltonian. With this time-dependent analysis, light-to-heavy-hole mixing tunnelling was found to be more effective than heavy-to-light-hole mixing tunnelling, and induces a significant spatial heavy-hole tunnelling. The mixing tunnelling, which has a higher oscillation frequency, also modulates the spatial tunnelling. In addition, the band-mixing effects slow down the HH and LH spatial tunnelling process the HH to LH mixing tunnelling while speeding up the LH to HH mixing tunnelling.

6 Acknowledgments

This work was supported by the National Science Council of R.O.C. under contracts 85-2215-E159-002 and 84-2121-M009-030.

7 References

1 LURYI, S.: *Solid State Commun.*, 1988, **65**, pp. 787
2 LURYI, S.: *IEEE J. Quantum Electron.*, 1991, **27**, pp. 54
3 DEVEAUD, B., CHOMETTE, A., CLEROT, F., AUVRAY, P., REGRENY, A., FERREIRA, R., and BASTARD, G.: *Phys. Rev.*, 1990, **B42**, pp. 7021
4 OBERLI, D.Y., SHAH, J., DAMEN, T.C., WU, C.T., CHANG, T.Y., MILLER, D.A.B., HENRY, J.E., KOPF, R.F., SAUER, N., and DI-GIOVANNI, A.E.: *Phys. Rev. B*, 1989, **40**, pp. 3028
5 SHIMIZU, N., FURUTA, T., WAHO, T., and MIZUTANI, T.: *Jpn. J. Appl. Phys.*, 1990, **L29**, pp. 1757
6 TARUCHA, S., PLOOG, K., and KLITZING, K.V.: *Phys. Rev.*, 1990, **B36**, pp. 4558
7 LEO, K., SHAH, J., GÖBEL, O., DAMEN, T.C., SCHMITT-RINK, S., and SCHÄFER, W.: *Phys. Rev. Lett.*, 1991, **66**, pp. 201
8 ROSKOS, H.G., NUSS, M.C., SHAH, J., LEO, K., MILLER, D.A.B., FOX, A.M., SCHMITT-RINK, S., and KÖHLER, K.: *Phys. Rev. Lett.*, 1992, **68**, pp. 2216
9 BRENER, I., PLANKEN, P.C.M., NUSS, M.C., LUO, M.S.C., CHUANG, S.L., PFEIFFER, L., LEAIRD, D.E., and WEINER, A.M.: *J. Opt. Soc. Am.*, 1994, **B11**, pp. 2457
10 LEO, K., SHAH, J., GORDON, J.P., DAMEN, T.C., MILLER, D.A.B., TU, C.W., and CUNNINGHAM, J.E.: *Phys. Rev.*, 1990, **B42**, pp. 7065
11 FERREIRA, R., and BASTARD, G.: *Europhys. Lett.*, 1989, **10**, pp. 279
12 TING, D.Z.Y., YU, E.T., and MCGILL, T.C.: *Phys. Rev.*, 1992, **B45**, pp. 3576
13 XIA, J.B.: *Phys. Rev.*, 1988, **B38**, pp. 8365
14 NORRIS, T.B., VODJDANI, N., VINTER, B., COSTARD, E., and BÖCKENHOFF, E.: *Phys. Rev.*, 1991, **B43**, pp. 1867
15 NIDO, M., ALEXANDER, M.G.W., RÜHLE, W.W., and KÖHLER, K.: *Phys. Rev.*, 1991, **B43**, pp. 1839
16 ROUSSIGNOL, P.H., VINATTIERI, A., CARRARESI, L., COLOCCI, M., and FASOLINO, A.: *Phys. Rev.*, 1991, **B44**, pp. 8873
17 PLANKEN, P.C.M., NUSS, M.C., BRENER, I., GOSSEN, K.W., LUO, M.S.C., CHUANG, S.L., and PFEIFFER, L.: *Phys. Rev. Lett.*, 1992, **69**, pp. 3800
18 JUANG, C., KUHN, K.J., and DARLING, R.B.: *Phys. Rev.*, 1990, **B41**, pp. 12047
19 JUANG, C.: *Phys. Rev.*, 1991, **B44**, pp. 10706
20 JUANG, C., CHEN, P.A., and CHANG, C.Y.: *Phys. Rev.*, 1993, **B47**, pp. 4563
21 CHUANG, S.L.: *Phys. Rev.*, 1991, **B43**, pp. 9649